Available online at www.sciencedirect.com
ScienceDirect
Journal of the European Ceramic Society 27 (2007) 4727–4735
www.elsevier.com/locate/jeurceramsoc

Laser densification of alumina powder beds generated using aerosol assisted spray deposition

Yiquan Wu [a,*], Jing Du [b], Kwang-Leong Choy [b], Larry L. Hench [a]

[a] *Department of Materials, Imperial College London, London SW7 2AZ, UK*
[b] *School of Mechanical, Materials and Manufacturing Engineering, University of Nottingham, NG7 2RD, UK*

Received 22 July 2006; received in revised form 29 January 2007; accepted 23 February 2007
Available online 2 May 2007

Abstract

Layered manufacturing involves a range of techniques in which objects can be constructed in a laminated form. Therefore, the deposition technique is a critical part of direct-layered fabrication technologies. In this paper, aerosol assisted spray deposition has been applied to generate spraying of a suspension to prepare powder beds for subsequent selective laser sintering. First, an investigation on preparation of the alumina suspension by adding polyacrylic acid dispersant is presented. An emphasis has been given to identify the most effective dispersant to enhance the dispersibility of alumina suspension for aerosol spraying deposition. Subsequently, a laser has been used to selectively densify the alumina powder beds to produce ceramics. The effects of the laser processing parameters such as scanning speed, power and beam size on the microstructural evolution of the powder beds are investigated and discussed. Also, a laser densification mechanism is also proposed and discussed.

Keywords: Sintering; Al_2O_3; Spray deposition

1. Introduction

Alumina ceramics can be found in a wide variety of applications such as filters, thermal insulation components, and dielectric and biomedical devices due to their excellent mechanical, thermal and optical properties.[1–4] Therefore, a number of processing techniques have been developed for preparing alumina ceramics with a desired shape, such as ink-jet printing, laminated object manufacturing, fused deposition processing and selective laser sintering.[5–8] Among these methods, selective laser sintering is one of the main techniques involving the use of a laser for materials processing, which can generate a ceramic part by densifying successive layers of powder materials. Densification is obtained by fusing or sintering selected areas of the powder layers using a laser beam. Short processing time, flexibility in operation and economy are the main advantages of laser sintering.[9,10]

Selective laser sintering requires a powder deposition process, which can apply successively thin layers of powder before the layers are sintered by a laser beam. Several studies have been devoted to develop suitable methods to prepare smooth powder layers.[11–13] In this work, aerosol assisted spray deposition with unique characteristics was used for the fabrication of alumina powder beds; the laser was then used to densify the powder beds to form ceramics. This technique is considered as a promising method for the direct fabrication of ceramics because aerosol spray deposition is a well-developed technique for preparing uniform powder beds with controllable microstructures.[14] Therefore, the study of laser densification of powder beds is necessary in order to explore and broaden the applications of laser-assisted ceramic fabrication. The research presented here includes the preparation of alumina powder beds via aerosol assisted spray deposition, laser densification of powder beds and microstructure characterization.

In order to deposit uniform alumina powder beds the ceramic suspension should be homogeneous, stable and well dispersed. Generally, the suspension can be dispersed by electrostatic, steric or electrosteric stabilization mechanisms.[15–17] In this paper, the stability of suspensions was primarily assessed using UV–vis absorption with an emphasis on identifying the most

* Corresponding author. Current address: Pratt School of Engineering, Duke University, 27708, USA. Tel.: +1 919 684 4587; fax: +1 919 660 5409.
E-mail address: yiquan.wu@duke.edu (Y. Wu).

0955-2219/$ – see front matter © 2007 Elsevier Ltd. All rights reserved.
doi:10.1016/j.jeurceramsoc.2007.02.219

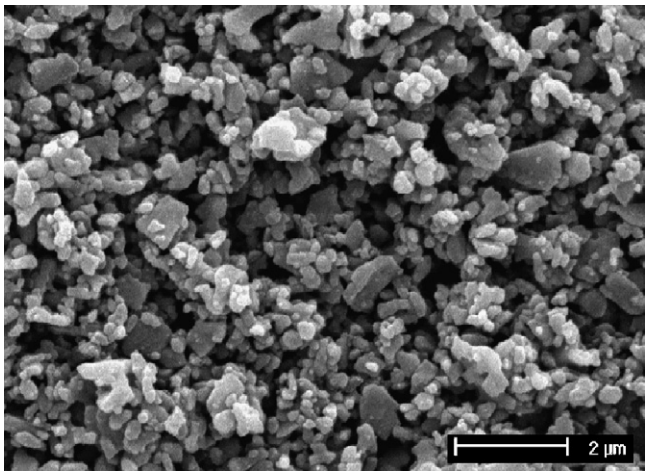

Fig. 1. SEM micrograph of starting alumina powder.

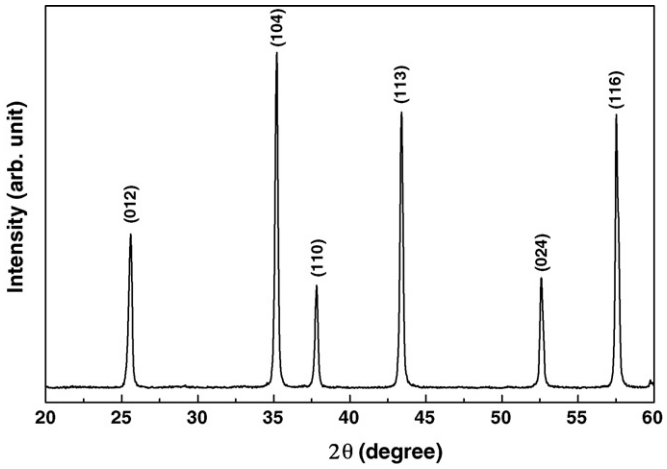

Fig. 3. XRD patterns of starting alumina powder.

effective dispersant necessary to enhance the dispersibility of alumina suspensions suitable for use in the electrospraying process. Laser densification of ceramics is a complicated process and the microstructure features are mainly influenced by the processing parameters, which include laser power, laser scanning speed and laser beam size.[18] This research aimed to understand the effects of laser processing parameters on the microstructural evolution of laser-densified alumina powder beds, and to optimize the laser parameters for laser fabrication.

2. Experimental

Alumina suspensions were prepared by adding 5 wt% alumina powder (Alcan Chemicals) to an ethanol solvent (Aldrich, 99.5%) with a different content PAA dispersant (Aldrich, M_w 2000). Fig. 1 shows a SEM (scanning electron microscope, Philips XL-30) image of the starting alumina powder. Particle size and distribution of alumina powder was analyzed using a particle size analyser (Malvern Zatasizer Nano S) and shown in Fig. 2. It can be seen from Fig. 2 that the alumina powder has a unimodal distribution with an average grain size of about 0.45 μm, which is in good agreement with the SEM micrograph analysis. An X-ray diffraction (XRD, Philips PW 1710) spectrometer with Cu Kα radiation was used to characterize the starting materials. The XRD patterns in Fig. 3 shows that the starting alumina powder is pure α-alumina phase. Table 1 summarise the chemical composition of the alumina powder.

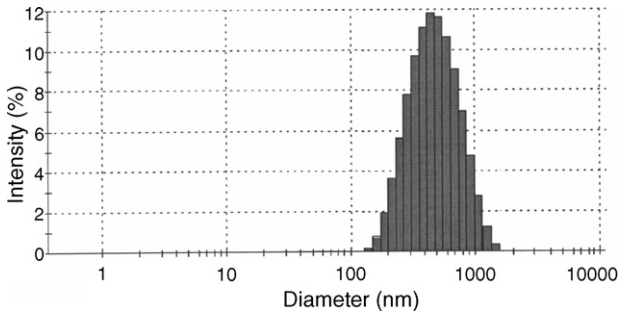

Fig. 2. Particle size distribution of starting alumina powder.

Table 1
Chemical analysis of starting alumina powder (wt%)

Al_2O_3	>99.8
Na_2O	0.04
SiO_2	0.01
Fe_2O_3	0.01
CaO	0.01
MgO	0.05

The suspensions were subjected to ultrasonic agitation for 30 min and then stirred with a magnetic stirrer for 24 h at room temperature. The amount of PAA absorbed on the alumina particles was analyzed using a UV–vis spectrophotometer (Biochrom Libra S22). The absorbed amount was determined by calculating the difference between the original PAA concentration in the suspension and the residual PAA concentration in the supernatant. The viscosity of suspension was determined using a concentric cylinder viscometer at 25 °C (Rheostress RS150L, Haake, Germany). First, a uniform layer of alumina powder was deposited using aerosol assisted spray deposition. Alumina suspension was delivered at a controlled rate to the electrostatic atomiser to generate a charged aerosol droplet. The deposition temperatures were varied from 60 °C to 120 °C. Fig. 4 shows a schematic diagram of aerosol spray deposition apparatus.

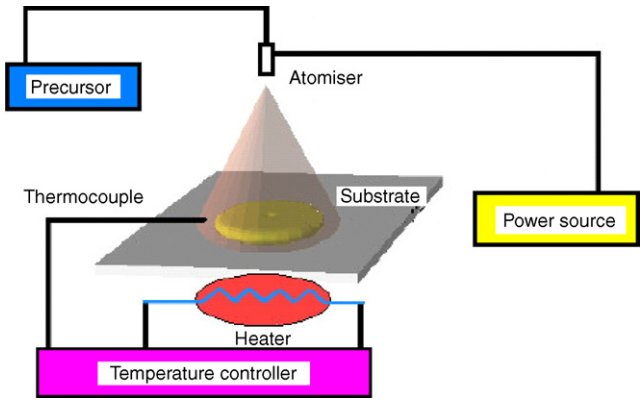

Fig. 4. Schematic illustrations of the aerosol deposition apparatus.

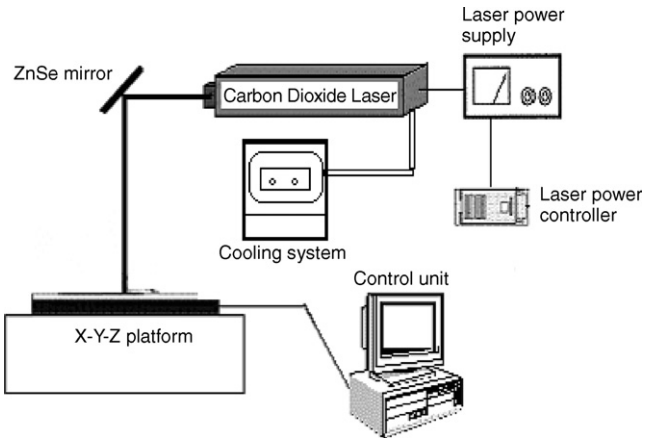

Fig. 5. Schematic diagram of setup of laser densification apparatus.

Subsequently a carbon dioxide laser was scanned on the powder bed to produce ceramics. For laser processing of materials, three important processing parameters were studied: laser power P (W), scanning speed V (mm s^{-1}) and laser beam size D (mm). Other criteria that were used were laser power density, E (W mm^{-2}), defined as $E = 4P/(\pi D^2)$, and laser energy density, J (J mm^{-2}), defined as $J = P/VD$. Fig. 5 shows a schematic diagram of setup of the laser processing system. SEM was used to characterize the microstructure of alumina powder beds prepared via aerosol spraying deposition and the laser-densified alumina powder beds. The pore size and size distribution of powder beds were measured from the SEM micrographs.

3. Results and discussion

3.1. Preparation of alumina powder beds

In order to achieve well-dispersed alumina suspensions, a UV–vis spectrophotometer was used for the suspension analysis to obtain an optimum PAA content. The absorption of PAA onto the alumina particle surface in the suspension can be calculated by determining the difference between the initial PAA concentration in suspension and the residual PAA concentration in supernatant. The concentration of PAA in supernatant is related to the intensity of UV absorption spectra of PAA at a wavelength of 267 nm. Fig. 6 shows the absorption spectra of PAA in a range of 0.0078–0.5 wt% as a function of the wavelength for 0 wt% alumina loading suspension. The intensities of UV absorption spectra of PAA were decreased when the PAA concentration was diluted from 0.5 wt% to 0.0078 wt%. When the PAA concentration was 0.0078 wt%, the intensity of the UV absorption spectrum was approximately zero. The results demonstrate that the intensities of UV absorption spectra at a wavelength of 267 nm are linearly dependent on the PAA concentration in the solutions. Fig. 7 shows the UV absorption spectra of the suspensions with an alumina loading of 5 wt% in a range of 0.2–0.5 wt% PAA. The absorption spectra show that the intensity of UV at the wavelength of 267 nm is decreased as the PAA content is decreased from 0.5 wt% to 0.2 wt%. The spectra shows that when 0.2 wt% PAA is added into an alumina

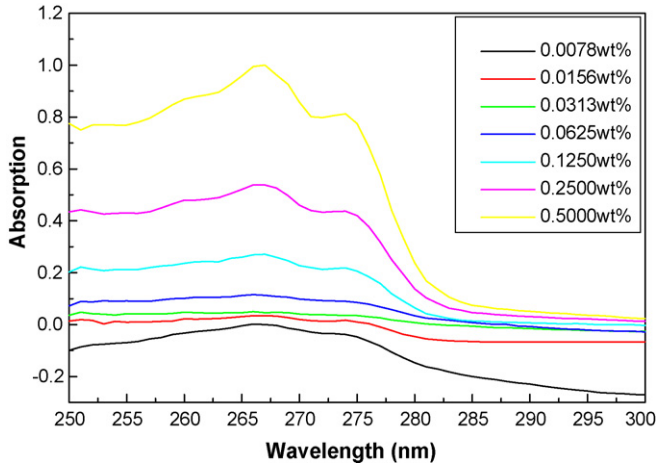

Fig. 6. Absorption spectra of different PAA content for 0 wt% alumina loading.

suspension, the intensity of UV absorption at the wavelength of 267 nm in the supernatant is equal to zero, which demonstrates that the PAA concentration in the supernatant is approximately equal to zero. It can be concluded that the PAA is absorbed on the alumina particle surface completely at a content of 0.2 wt%. Full absorption is considered to be the condition for an optimal PAA concentration, corresponding to full monolayer coverage of the particle surface by PAA. The absorption of PAA on the particle surface should be maintained when a repulsive interaction is expected to stabilize the suspension. Therefore, the optimum amount of PAA that produces a well-dispersed suspension is 0.2 wt% of alumina loading.

Gravity sedimentation tests were also performed by pouring the as-prepared suspensions into glass cylinders and leaving them to stand undisturbed for 24 h. A profile of the suspension height from cylinder bottom with PAA content in a range of 0.1–0.5 wt% for different alumina loading is shown in Fig. 8. The height indication is the height of alumina suspension from the cylinder bottom. The suspension height from bottom is highest at a PAA concentration of 0.2 wt%. Above a concentration of 0.2 wt%, the suspension height decreases with an increase of PAA content. It confirms that the optimum PAA concentration is 0.2 wt% of alumina loading to obtain a well-dispersed

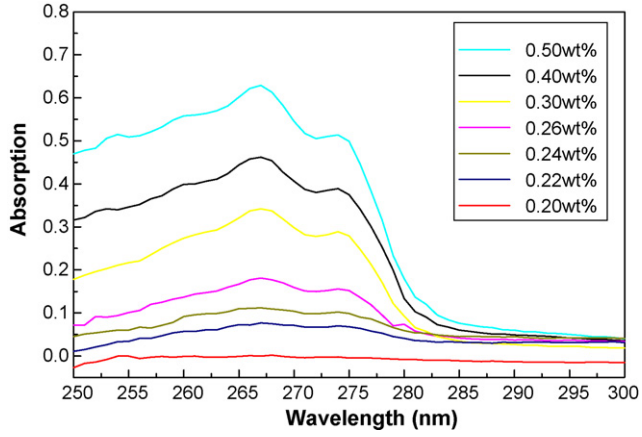

Fig. 7. Absorption spectra of different PAA content for 5 wt% alumina loading.

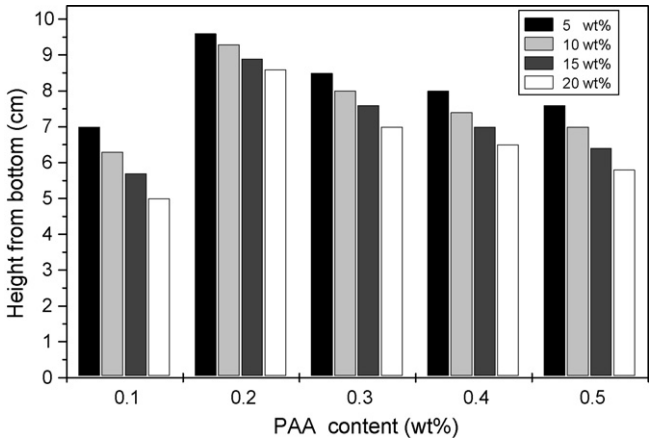

Fig. 8. Sedimentation of alumina suspensions with different PAA contents.

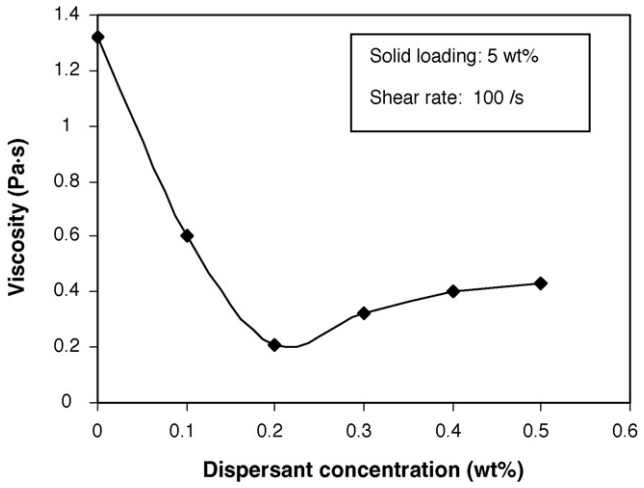

Fig. 9. Viscosity of 5 wt% alumina suspension as a function of PAA concentration.

suspension. Excessive PAA slightly decreases the dispersion of the suspension. It is attributed to that the bridge flocculation is the main reason for the decreased dispersion of suspension.[19,20] The experimental results also reveal that the suspension height from bottom is decreased with an increased alumina loading from 5 wt% to 20 wt%. This is believed to the reason that the distance between the particles become short in the alumina suspension with a high alumina concentration, which easily results in a bridge flocculation.[21] The bridge flocculation causes the sedimentation of alumina particles, which is revealed through the variation of suspension height. By adding an optimum content of PAA, a well-dispersed alumina suspension with different alumina loading can be obtained.

Fig. 9 shows the viscosities of alumina suspensions with 5 wt% loading as a function of PAA concentration. The PAA concentrations are varied from 0 wt% to 0.5 wt% of alumina loading. The results show that the viscosities of suspensions apparently depend on the PAA concentration. At a low concentration, the viscosity decreases with increasing the PAA concentration, reaching a minimum value at approximately 0.2 wt% of alumina loading. However, addition of excess PAA increases the viscosity of suspension linearly with increasing PAA concentration. It is believed that a bridging flocculation is formed in suspension and become significant at high PAA concentration, because a network structure develops by the bridging effect retarding the sliding of particles and increasing the viscosity of suspension.[19,21] From Fig. 9, it is concluded that an optimum concentration of PAA was 0.2 wt%. The absorption of PAA on the particle surface should be maintained if a repulsive interaction is expected to stabilize the suspension. At a low content of dispersant, the surfaces of the particles is partially covered by PAA and an electric charge is formed to act as repulsive force, which then repels the particles from each other. This in turn causes a decrease in the viscosity of suspension. When the PAA concentration increases over the equilibrium concentration, the excessive PAA dispersant also absorbs onto the surface of particles already fully covered by PAA. In this case, the excessive PAA easily forms bridging between neighbouring particles, which in turn increases the viscosity of suspension. Full absorption is considered to be the condition for maximum PAA concentration, corresponding to full monolayer coverage of the particle surface by PAA. Therefore, the optimum amount of PAA that produces the lowest viscosity of suspension is 0.2 wt% of alumina loading in this experiment.

Fig. 10 shows a SEM micrograph of alumina powder beds prepared via aerosol assisted spray deposition at 60 °C using

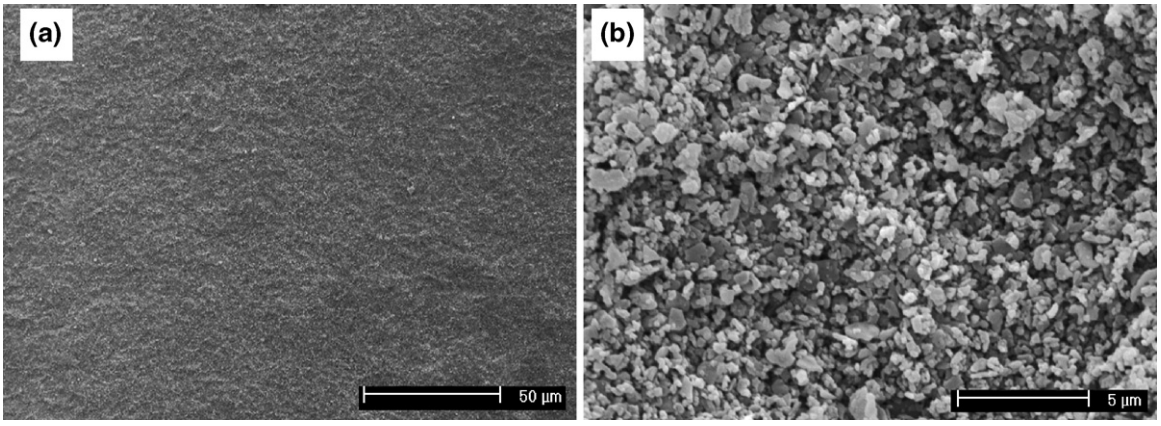

Fig. 10. SEM micrographs of alumina powder bed prepared using 5 wt% alumina loading suspension: (a) low magnification and (b) high magnification.

5 wt% alumina suspension. The SEM image shows that the powder bed had a uniform and smooth surface, which is very important for laser densification. A high-magnification SEM micrograph in Fig. 10 indicates that the particles with an average size of approximately 0.45 μm were closely packed together to form a uniform powder bed with a relatively high density. The average pore size was approximately 0.9 μm and the pores were distributed in the powder beds homogeneously. The aerosol assisted spray deposition is a process where the precursor at the tip of an electrostatic atomiser breaks into sprayed charged aerosol droplets. Spraying of alumina suspension in a stable cone-jet mode can produce mono-dispersed droplets in a controllable way, which is advantageous for obtaining the desired powder beds with a uniform and well-controlled microstructure.[22]

3.2. Laser densification of alumina powder beds

3.2.1. Effect of laser power

Fig. 11 shows SEM micrographs for the microstructures of laser-densified alumina powder beds at a scanning speed of 4.0 mm/s and a laser beam size of 2.0 mm using various laser powers from 10 W to 60 W. At a laser power of 10 W, the SEM micrograph in Fig. 11(a) shows that the laser-densified powder bed consisted of small grains with an average size of 0.5 μm. The average pore size was approximately 1.0 μm. The grains were partially bonded to each other to form the sintering neck. At a laser power of 20 W, the agglomerated clusters were sintered further and coarsened significantly to form irregular grains in a size range of 0.5–1.0 μm, as shown in Fig. 11(b). Fig. 11(c) shows that large grains with irregular and spherical morphologies were formed on the laser-scanned powder bed when a laser power of 40 W was used indicating an increase in the densification of powder beds. It is believed that at a laser energy density of 5.0 J mm^{-2} obtained using a laser power of 40 W a liquid-phase with a low viscosity was formed, which resulted in the formation of dense microstructure and spherical grains.[23] The SEM micrograph in Fig. 11(d) shows that further increasing the laser power to 60 W caused the powder bed to be densified dramatically and a smooth microstructure with small pores was formed. The liquid-phase sintering was dominant and the alumina particles recrystallized into larger grains, which had an irregular shape due to the fast melting–crystallization–solidification process in the laser densification.

3.2.2. Effect of laser scanning speed

Fig. 12 shows SEM micrographs for the morphologies of laser-sintered powder beds using a laser beam size of 2.0 mm, a laser power of 65 W and a laser scanning speed of 2 mm/s and 4 mm/s, respectively. To increase the densification of powder beds, a low scanning speed of 2 mm/s was chosen in order to obtain a high laser energy density. Laser densification at a laser scanning speed of 4.0 mm/s produced a sintered and dense microstructure. The initial stage of sintering occurred and sin-

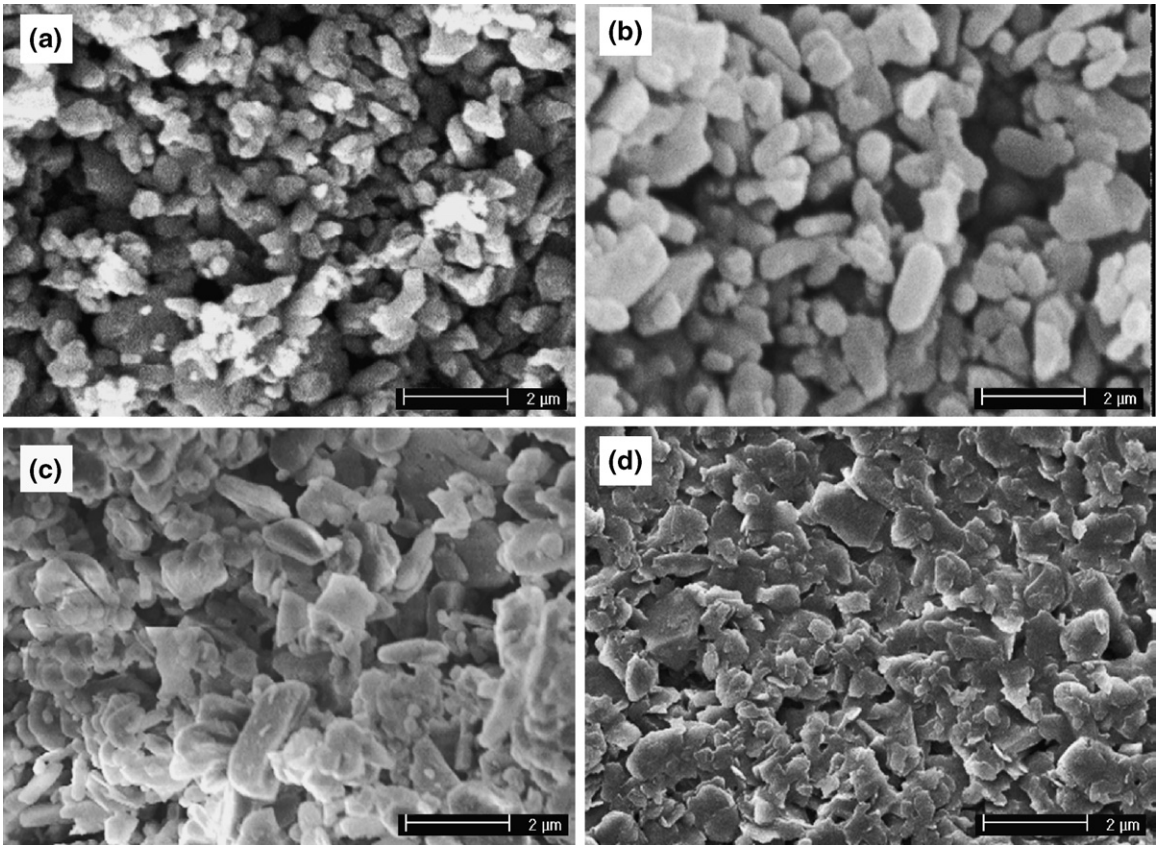

Fig. 11. SEM micrographs of alumina powder beds densified using laser powers of (a) 10 W, (b) 20 W, (c) 40 W and (d) 60 W.

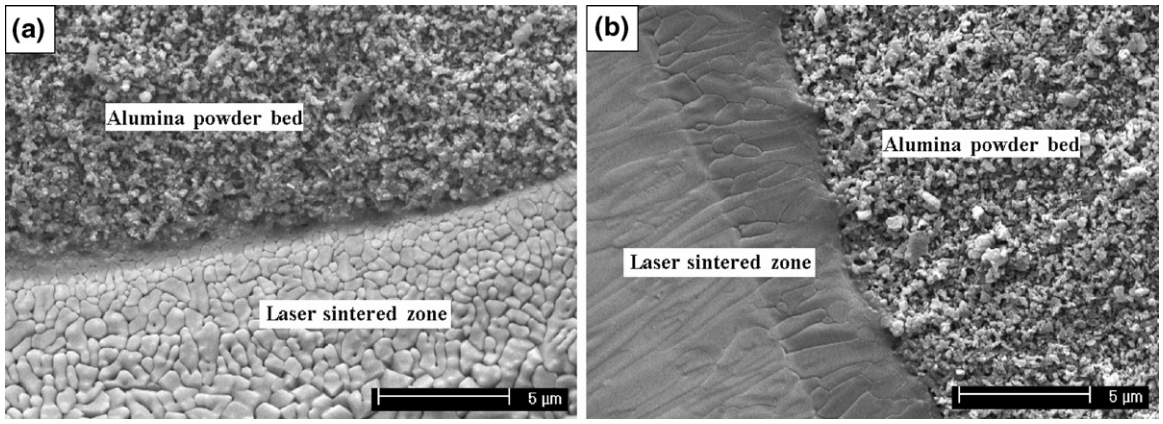

Fig. 12. SEM micrographs of powder beds densified using laser scanning speeds of (a) 4 mm/s and (b) 2 mm/s.

tering necks of powder particles were formed. The grains, with an average size of 1.2 μm and small pores with an average size of approximately 0.15 μm around the grains, could be identified from Fig. 12(a). The laser scanning speed of 4 mm/s resulted in a laser energy density of 8.2 J mm^{-2}, which can improve the laser densification but was not high enough to fully densify the powder bed. The interface between the laser-sintered part and the unsintered part can clearly be seen from the SEM images and the surface of both parts was smooth. With a decrease of laser scanning speed to 2.0 mm/s, melting phenomena occurred in the laser-scanned powder bed and the particles were fused together so that the individual particles could not be clearly identified from Fig. 12(b). A low laser scanning speed would result in a high laser energy density and a high temperature accordingly, which promoted the laser densification of powder beds.

3.2.3. *Effect of laser beam size*

Fig. 13 shows the microstructural development of powder beds densified with a laser scanning speed of 4.0 mm/s and a laser power of 68 W using different laser beam sizes: 2.5 mm, 2.0 mm and 1.5 mm, respectively. From the SEM image in Fig. 13(a), it was observed that spherical particles were formed and bonded to each other when a laser beam with a size of 2.5 mm was used. Coalescence of particles was thermally activated when

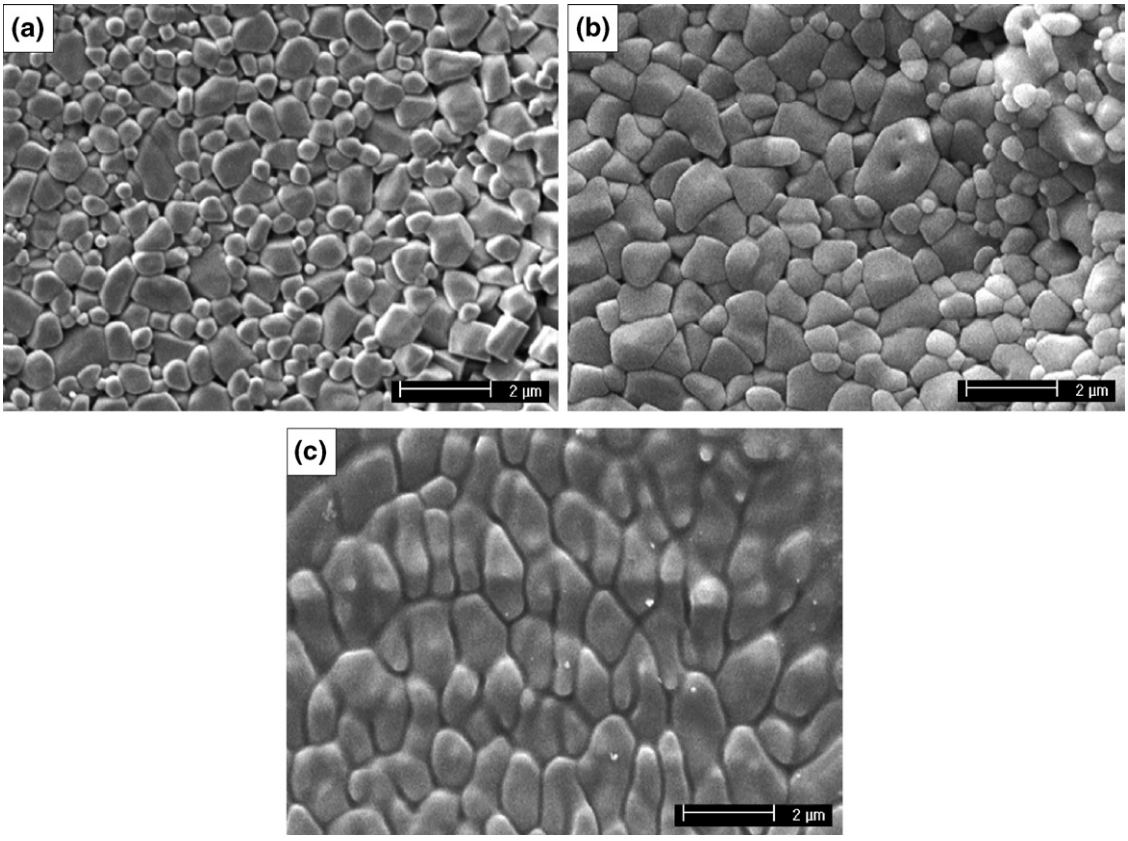

Fig. 13. SEM micrographs of alumina powder beds densified using laser beam sizes of (a) 2.5 mm, (b) 2.0 mm and (c) 1.5 mm.

Table 2
Optimized laser parameters for preparing alumina ceramics

D (mm)	2.0
V (mm/s)	4.0
P (W)	72
P/VD (J mm^{-2})	9.0

laser energy of 6.8 J mm^{-2} was obtained at a laser beam size of 2.5 mm, but the laser energy density was not sufficient to densify powder beds fully. When the laser beam size was reduced to 2.0 mm the laser energy density was increased to 8.5 J mm^{-2} and the laser densification of powder beds was promoted as shown in Fig. 13(b). From the SEM micrograph it can be seen that small grains became spares and large grains dominate the image. The average grain size was approximately 1.2 μm. The formation of small spherical, regular particles and the smooth grain surface indicated a liquid-phase was formed.[24] The microstructure of powder beds after laser densification using a laser beam size of 1.5 mm is shown in Fig. 13(c). The SEM micrograph shows that plate-like grains were formed in the powder beds densified by laser irradiation at a laser energy density of 11.3 J mm^{-2}. It is concluded that laser densification of powder beds can be increased by decreasing the laser beam size from 2.5 mm to 1.5 mm, because the laser energy density is increased from 6.8 J mm^{-2} to 11.3 J mm^{-2}.

3.3. Fabrication of alumina ceramics

Fig. 14 shows a digital image of the alumina ceramics fabricated using a laser-assisted fabrication method, in which laser densification was performed on the powder beds prepared using aerosol assisted spray deposition. The selected processing parameters based on the results are listed in Table 2. The SEM micrographs of surface and cross-section microstructure of the laser-densified alumina ceramics are shown in Fig. 15. The alumina prepared using laser-assisted fabrication was very dense, which revealed that the green layer was fully densified by the laser. The grain sizes were in the range of 0.3–2.0 μm, with an average grain size of 1.5 μm. Very few pores occurred in the triple grain-boundary.

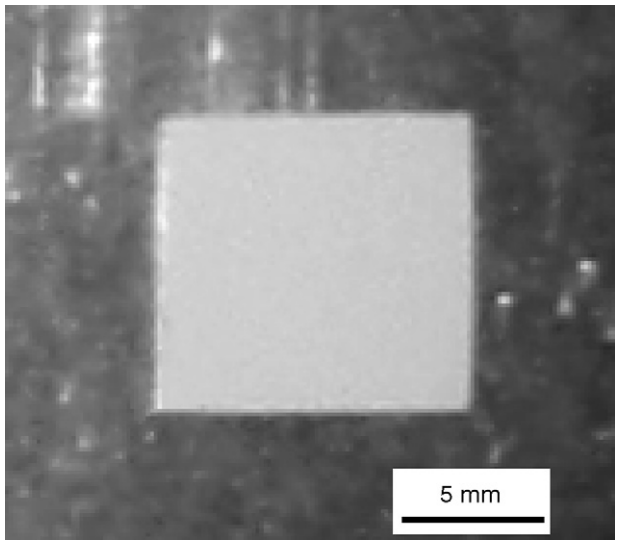

Fig. 14. Digital image of laser-densified alumina ceramic.

3.4. Laser densification mechanism of alumina powder bed

In laser densification of alumina powder beds the energy is delivered point-by-point in a short period of time, and the interaction between laser beam and particles depends on the laser scanning speed. Under a short laser-irradiation of the powder bed, the particle bonding and sintering must be rapid and thus solid-phase sintering, which requires a long diffusion time, does not seem to be feasible in selective laser sintering.[25,26] Melting/solidification and liquid-phase sintering are the feasible mechanisms for laser densification of alumina powder beds. In practice, laser sintering of alumina powder beds may be considered in three stages[27]: (1) initial sintering up to a eutectic formation of liquid-phase. The eutectic phase systems include Al_2O_3–SiO_2, CaO–Al_2O_3–SiO_2, Fe_2O_3–Al_2O_3–SiO_2 and Na_2O–Al_2O_3–SiO_2, which result from the impurities in the starting alumina powder listed in Table 1; (2) liquid-phase sintering allowing the liquid-phase to spread; (3) liquid–solid phase bonding and sintering during the period of cooling after laser irradiation.

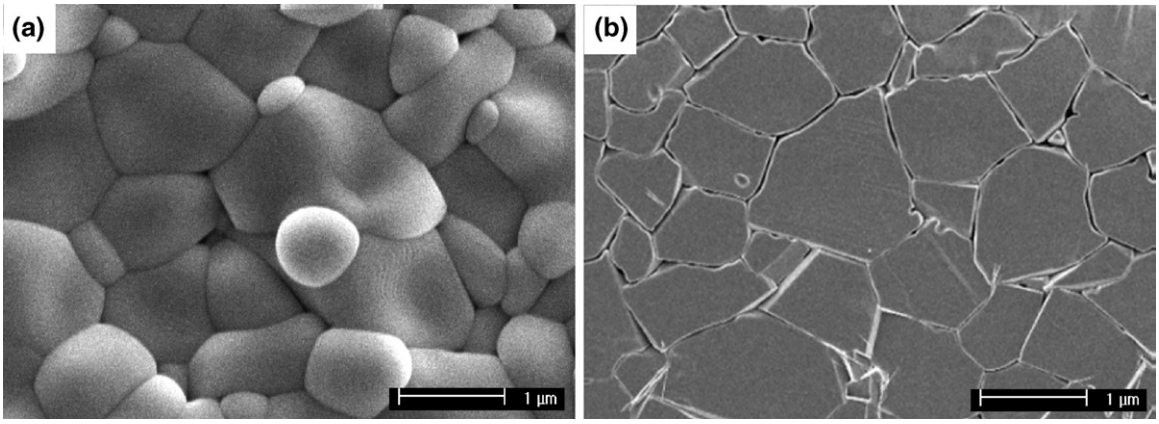

Fig. 15. SEM micrographs of ceramic alumina prepared by laser-densified powder bed: (a) surface and (b) cross-section.

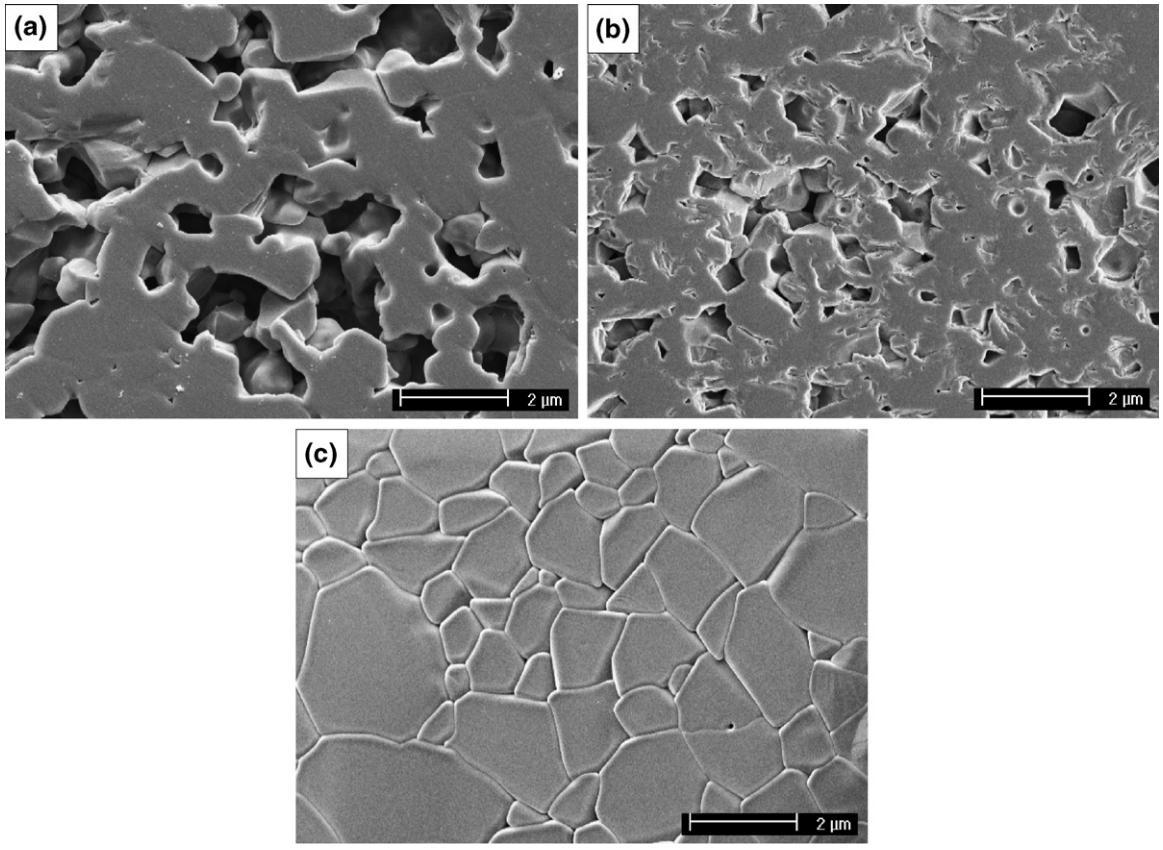

Fig. 16. Cross-section SEM micrographs of alumina powder beds densified using laser energy densities of (a) 4.0 J mm^{-2}, (b) 7.0 J mm^{-2} and (c) 8.5 J mm^{-2}.

The laser processing parameters have an influence on the laser energy density and are helpful in understanding the laser densification mechanism because the densification of powder beds is a function of laser energy density. The SEM cross-section micrographs of the alumina powder beds densified using different laser energy densities are shown in Fig. 16(a)–(c). The laser processing parameters are listed in Table 3. At a laser energy density of 4.0 J mm^{-2}, the alumina particles are sintered and bonded together at points of contact. The individual particles and the sintering necks at points of contact between particles can be identified from the SEM image in Fig. 16(a). A small amount of liquid-phase resulted from the low eutectic impurities is believed to be formed at a measured temperature of 1123 °C under a laser energy density of 4.0 J mm^{-2}, because the formation of spherical grains is an indication of liquid-phase formation during the sintering process. Fig. 16(b) shows that as the laser energy density is increased to 7.0 J mm^{-2}, the alumina particles are sintered to form larger grains through liquid-phase sintering, which is confirmed by the formation of a smooth surface of grains and the sintering necks.[28] The sintering necking phenomenon between the grains is obvious, because a laser energy density of 7.0 J mm^{-2} results in an increase of sintering temperature on alumina powder beds, and thus more liquid-phase is formed. The rounding of the edges of individual particles also indicates that liquid-phase sintering has occurred during the laser densification of powder beds. Fig. 16(c) shows that when the laser energy density is increased to 8.5 J mm^{-2}, the alumina powder bed is densified completely. The morphology of the particles evolves into a spherical shape and the surface become smoother after the laser sintering process has occurred, which reveals the existence of liquid-phase. From the viewpoint of sintering, the densification rate in a liquid-phase sintering through viscous flow and rearrangement is mainly determined by the wetting and viscosity of a body composed of solid particles held together by a liquid-phase. Therefore, the sintering rate during liquid-phase sintering is determined by the kinetics of liquid–solid transformation, which are several orders of magnitude faster than the solid-phase diffusion which occurs in solid-phase sintering.[24] It has been concluded that the advantage of liquid-phase sintering during laser densification of powder beds is a fast initial bonding and sintering caused by capillary forces of liquid-phase in the alumina powder beds.

Table 3
Different laser energy densities used for densifying alumina powder beds

Parameters	D (mm)	V (mm/s)	P (W)	P/VD (J mm^{-2})
a	2.0	4.0	32	4.0
b	2.0	4.0	56	7.0
c	2.0	4.0	68	8.5

4. Conclusions

The properties of alumina suspensions were characterized with regard to viscosity and PAA concentration in this experiment. PAA was an effective dispersant for preparing

a well-dispersed alumina suspension by introducing an electrosteric stabilization to prevent particle agglomeration. The optimum content of PAA was 0.2 wt% of alumina loading when a full coverage of particles without bridging was achieved. The addition of excessive PAA would form bridging between the alumina particles, which accelerated powder agglomeration and increased the suspension viscosity. The aerosol assisted spray deposition via an electrostatic atomiser has been used to generate droplets of alumina suspension to prepare alumina powder beds. Laser densification of alumina powder beds was studied using laser powers of 10–70 W, laser scanning speeds of 2–4 mm/s and laser beam sizes of 1.5–2.5 mm. With increasing laser power, the microstructure of laser-sintered alumina powder beds varied from open/closed pores to a fully densified microstructure. Decreasing laser scanning speed or laser beam size would promote the laser densification of alumina powder beds due to an increase in the laser energy density. During the laser densification of alumina powder beds, submicron particles in the starting materials were melted to form liquid-phase under the laser irradiation at a laser power of 40 W. The liquid-phase facilitates the sintering and densification of alumina powder beds through liquid-phase sintering because the liquid-phase flows and fills the pores between the micrometer alumina particles and then solidifies to form a dense microstructure. The experimental results showed that the final microstructure and quality of the laser-sintered alumina powder beds depended strongly on the laser parameters, such as laser power, laser scanning speed and laser beam size. The optimum laser densification parameters include using a laser beam of 2 mm, a laser scanning speed of 4 mm/s and a laser power of 70 W in order to avoid under-densification and over-densification of the alumina powder beds. The established laser processing parameters and procedures will pave a way for making three-dimensional ceramic parts with controllable microstructures through solid freeform fabrication.

Acknowledgement

The authors Y. Wu and J. Du would like to acknowledge the financial support provided under the Overseas Research Scholarship (ORS) Scheme from UK Government for their PhD study.

References

1. Haanappel, V., Vendel, D., Metselaar, H., Corbach, H., Fransen, T. and Gellings, P., The mechanical properties of thin alumina films deposited by metal-organic chemical vapour deposition. *Thin Solid Films*, 1995, **254**, 153–163.
2. Craig, B. and Francis, L., Alumina/epoxy interpenetrating phase composite coatings. I. Processing and microstructural development. *J. Am. Ceram. Soc.*, 1998, **81**, 3109–3116.
3. Doll, T., Vuckovic, J., Hochberg, M. and Scherer, A., Low-energy electron beam focusing in self-organized porous alumina vacuum windows. *Appl. Phys. Lett.*, 2000, **76**, 3635–3637.
4. Kinsho, M., Saito, Y., Nishizawa, D. and Michizono, S., 2.5 Mev electron irradiation effects of alumina ceramics. *J. Nucl. Mater.*, 2003, **318**, 307–312.
5. Cai, K., Guo, D., Huang, Y. and Yang, J. L., Solid freeform fabrication of alumina ceramic parts through a lost mould method. *J. Eur. Ceram. Soc.*, 2003, **23**, 921–925.
6. Marchi, C. S., Kouzeli, M., Rao, R., Lewis, J. A. and Dunand, D. C., Alumina–aluminum interpenetrating-phase composites with three-dimensional periodic architecture. *Scripta Mater.*, 2003, **49**, 861–866.
7. Zhang, Y. M., He, X. D., Han, J. C. and Du, S. Y., Ceramic green tape extrusion for laminated object manufacturing. *Mater. Lett.*, 1999, **40**, 275–279.
8. Donnchadha, B. and Tansey, A., A note on rapid metal composite tooling by selective laser sintering. *J. Mater. Process. Technol.*, 2004, **153–154**, 28–34.
9. Bourell, D. L., Marcus, H. L., Barlow, J. W. and Beaman, J. J., Selective laser sintering of metals and ceramics. *Int. J. Powder Metall.*, 1992, **28**, 369–381.
10. Berry, E., Brown, J. M., Connell, M., Craven, C. M., Efford, N. D., Radjenovic, A. *et al.*, Preliminary experience with medical applications of rapid prototyping by selective laser sintering. *Med. Eng. Phys.*, 1997, **19**, 90–96.
11. Holman, R. K., Cima, M. J., Uhland, S. A. and Sachs, E., Spreading and infiltration of inkjet-printed polymer solution droplets on a porous substrate. *J. Colloid Interf. Sci.*, 2002, **249**, 432–440.
12. Uhland, S. A., Holman, R. K., Morissette, S., Cima, M. J. and Sachs, E. M., Strength of green ceramics with low binder content. *J. Am. Ceram. Soc.*, 2001, **84**, 2809–2818.
13. Yang, S. F. and Evans, J. R. G., A dry powder jet printer for dispensing and combinatorial research. *Powder Technol.*, 2004, **142**, 219–222.
14. Wu, Y. Q., Choy, K. L. and Hench, L. L., Laser densification of TiO_2 films prepared by aerosol assisted vapour deposition. *Appl. Surf. Sci.*, 2005, **247**, 378–383.
15. Lewis, J. A., Colloidal processing of ceramics. *J. Am. Ceram. Soc.*, 2000, **83**, 2341–2359.
16. Kakui, T., Miyauchi, T. and Kamiya, H., Analysis of the action mechanism of polymer dispersant on dense ethanol alumina suspension using colloidal probe AFM. *J. Eur. Ceram. Soc.*, 2005, **25**, 655–661.
17. Sigmund, W. M., Bell, N. S. and Bergstrom, L., Novel powder-processing methods for advanced ceramics. *J. Am. Ceram. Soc.*, 2000, **83**, 1557–1574.
18. Simchi, A. and Pohl, H., Effects of laser sintering processing parameters on the microstructure and densification of iron powder. *Mater. Sci. Eng. A*, 2003, **359**, 119–128.
19. Bleier, A. and Westmoreland, C. G., In *Interfacial Phenomena in Biotechnology and Materials Processing*, ed. Y. A. Attia, B. M. Moudgil and S. Chander. Elsevier, Amsterdam, 1988, pp. 217–236.
20. Güngör, N., Alemdar, A., Atici, O. and Ece, I. O., The effect of SDS surfactant on the flow and zeta potential of bentonite suspensions. *Mater. Lett.*, 2001, **51**, 250–254.
21. Subbanna, M., Kapur, P. C. and Pradip, Role of powder size, packing, solid loading and dispersion in colloidal processing of ceramics. *Ceram. Int.*, 2002, **28**, 401–405.
22. Wu, Y. Q. and Choy, K. L., The microstructure of alumina coatings prepared by aerosol assisted spray deposition. *Surf. Coat. Technol.*, 2004, **180–181**, 436–440.
23. Kwon, O. H., *Liquid Phase Sintering: Ceramics. Encyclopedia of Materials: Science and Technology*. Elsevier Ltd., 2004, pp. 4597–4601.
24. Chiang, Y. M., Birnine, D. B. and Kingery, W. D., *Physical Ceramics: Principles for Ceramics Science and Engineering*. John Wiley & Sons Inc., New York, 1997, pp. 351–430.
25. Ragulya, A. V., Selective laser sintering. I. Principles, continual model. *Powder Metall. Met. Ceram.*, 1998, **37**, 356–364.
26. Ragulya, K. V., Stetsenko, V. P., Vereshchak, V. M., Klimenko, V. P. and Skorokhod, V. V., Selective laser sintering. II. Sintering multilayer refractory composites. *Powder Metall. Met. Ceram.*, 1998, **37**, 577–582.
27. Kruth, J. P., Mercelis, P., Vaerenbergh, J. V., Leuven, K. U., Froyen, L. L. and Rombouts, M., Binding mechanisms in selective laser sintering and selective laser melting. *Rapid Prototyping J.*, 2005, **11**, 26–36.
28. German, R. M., *Liquid Phase Sintering*. Plenum, New York, 1985.